ARTICLE

Check for updates

Deterioration mechanism of perovskite solar cells by operando observation of spin states

Takahiro Watanabe[1], Toshihiro Yamanari[2] & Kazuhiro Marumoto [ID] [1,3 ✉]

Perovskite solar cells are attractive because of their remarkably improved power conversion efficiency. In view of their application, however, it is important not only to increase the power conversion efficiency, but also to elucidate the deterioration mechanism. Here, we show operando direct observation of spin states in the cells using electron spin resonance, thereby investigating the operation and deterioration mechanisms from a microscopic viewpoint. By simultaneous measurements of solar cell characteristics and electron spin resonance, the spin states in the hole transport material spiro-OMeTAD are demonstrated to change in accordance with the device performance variation under operation. These variations are ascribed to the change of hole transport and to interfacial electric dipole layers. Reverse electron transfer from TiO_2 to the hole transport material layer is demonstrated under ultraviolet light irradiation, which decreases hole doping. Conducting such operando microscopic investigation will be useful to obtain further guidelines for improving the device performance and durability.

[1] Division of Materials Science, University of Tsukuba, Tsukuba, Ibaraki 305-8573, Japan. [2] Chemical Materials Evaluation and Research Base (CEREBA), Tsukuba, Ibaraki 305-8565, Japan. [3] Tsukuba Research Center for Energy Materials Science (TREMS), University of Tsukuba, Tsukuba, Ibaraki 305-8571, Japan. ✉email: marumoto@ims.tsukuba.ac.jp

Organic–inorganic hybrid perovskites have been actively studied because they can be easily fabricated by solution methods at low cost, and thus are useful for electronic devices such as solar cells[1–5], light-emitting diodes[6,7], and transistors[8,9]. Especially, perovskite solar cells have remarkably improved their power conversion efficiencies (PCEs) recently[10]. Today the PCE more than 25% has been reported, which is comparable to that of silicon solar cells, and the study for further PCEs improvement has been conducted[10]. Perovskite layers are utilized as photoactive layers in the cells, and wide light-absorption wavelength and long carrier lifetime have been reported[11–13].

Toward the practical application, it is important not only to increase the PCE but also to elucidate the deterioration mechanism of the devices. There are extrinsic and intrinsic factors which cause the performance deterioration. Extrinsic factors, for example, effects of moisture and oxygen, have been discussed[14–17], where the device performance deteriorates when oxygen in the air reacts with the perovskite layer during device operation[14], and the perovskite layer is decomposed by moisture[15]. In order to prevent such extrinsic deteriorations, the study under inert gas such as N_2 or Ar has been conducted[17]. The researches on the degradation by extrinsic factors have been actively performed. For the intrinsic factors, it has been discussed that iodine in the perovskite moves and causes defects during device operation[18]. However, there are still many unknown factors about the intrinsic deterioration. In order to clarify the factors of intrinsic degradation, it is important to elucidate the charge and defect states in the perovskite solar cells at a molecular level from a microscopic viewpoint; these states are often accompanied by spins.

For investigating microscopic properties such as spin states in electronic devices and their materials, electron spin resonance (ESR) spectroscopy is a useful technique[19–21]. ESR method is able to identify the molecules where charges with spins exist, and to determine the absolute number of spins by nondestructive operando observation of solar cells with high sensitivity and high precision[22,23]. For organic solar cells, operando ESR spectroscopy has shown that the charge accumulation and formation (or spin accumulation and formation) in molecules cause the deterioration of the device performance, where the origin of the intrinsic deterioration factor has been clarified[22–24]. ESR studies on perovskite solar-cell materials of a perovskite $CH_3NH_3PbI_3$ and hole transport materials (HTMs) 2,2′,7,7′-tetrakis-(N,N-di-p-methoxyphenylamine)9,9′-spirobifluorene (spiro-OMeTAD) or poly(3,4-ethylenedioxy-thiophene):poly(styrenesulfonate) (PEDOT:PSS) have been performed, which have demonstrated the microscopic observation of the effect of lithium bis(trifluoromethanesulfonyl) imide (Li-TFSI) doping on spiro-OMeTAD[25] and the charge transfer between $CH_3NH_3PbI_3$ and PEDOT:PSS[26]. However, detailed research for perovskite solar cells using operando ESR spectroscopy has not yet been conducted. Such research on spin states in perovskite solar cells from a microscopic viewpoint is important to elucidate the intrinsic deterioration mechanism in the devices.

Here, we study the intrinsic deterioration mechanism in perovskite solar cells with operando ESR spectroscopy from the microscopic viewpoint at a molecular level. The internal states such as spin states during device operation have been investigated by measuring the device characteristics, and ESR signals due to charges with spins at the same time using the same device. As a result, a clear change in the charge/spin states in the devices has been observed; the changes are correlated with the device performance. Such findings at the molecular level contribute the elucidations of not only the performance deterioration mechanism but also the operating mechanism in details, which would be

important for further improvements of performance and durability of perovskite solar cells.

Results and discussion

Device fabrication and characterization.
To perform highly sensitive and precise ESR measurements, it is necessary not only to seal the device in an ESR sample tube of a 3.5 mm inner diameter but also to improve ESR's signal-to-noise (S/N) ratio. For this purpose, a rectangular 3×20 mm^2 indium-tin-oxide (ITO) non-magnetic quartz substrate with a 2×10 mm^2 elongated active area was used. As a perovskite solar cell, we fabricated the device structure of quartz/ITO (150 nm)/compact TiO_2 (20 nm)/$CH_3NH_3PbI_3$ (300 nm)/spiro-OMeTAD (300 nm)/Au (100 nm) as shown in Fig. 1a. An energy diagram of the fabricated device is shown in Fig. 1b[27]. The reason for using this simple structure without a porous TiO_2 layer is that this work is the first operando ESR study of perovskite solar cells, and that we try to study the phenomena in the cells as simple as possible because the interfaces between porous TiO_2 and perovskite layers cause complicated phenomena such as hysteresis behavior in current–voltage characteristics. The layered samples of quartz/ITO/spiro-OMeTAD and quartz/ITO/compact TiO_2/$CH_3NH_3PbI_3$/spiro-OMeTAD were
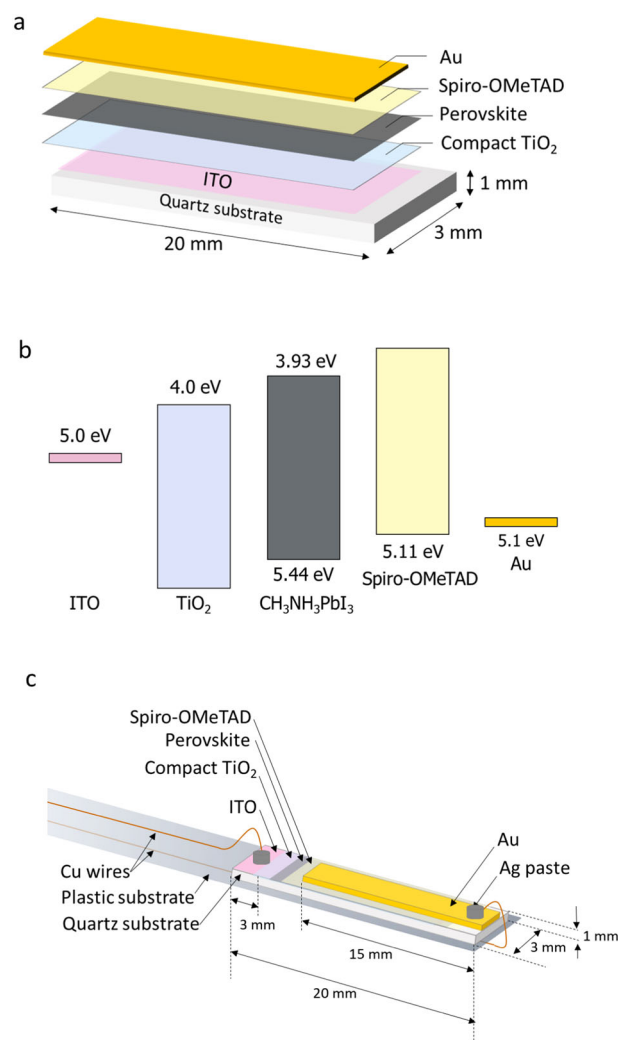
Fig. 1 Schematic of a perovskite solar cell and the energy-level diagram. a Schematic structure of the perovskite solar cell of quartz/ITO/compact TiO_2/$CH_3NH_3PbI_3$/spiro-OMeTAD/Au used in this study. **b** Energy diagram for each component of the cell. **c** Schematic structure of electrical contacts and wires of the perovskite solar cell in an ESR sample tube.
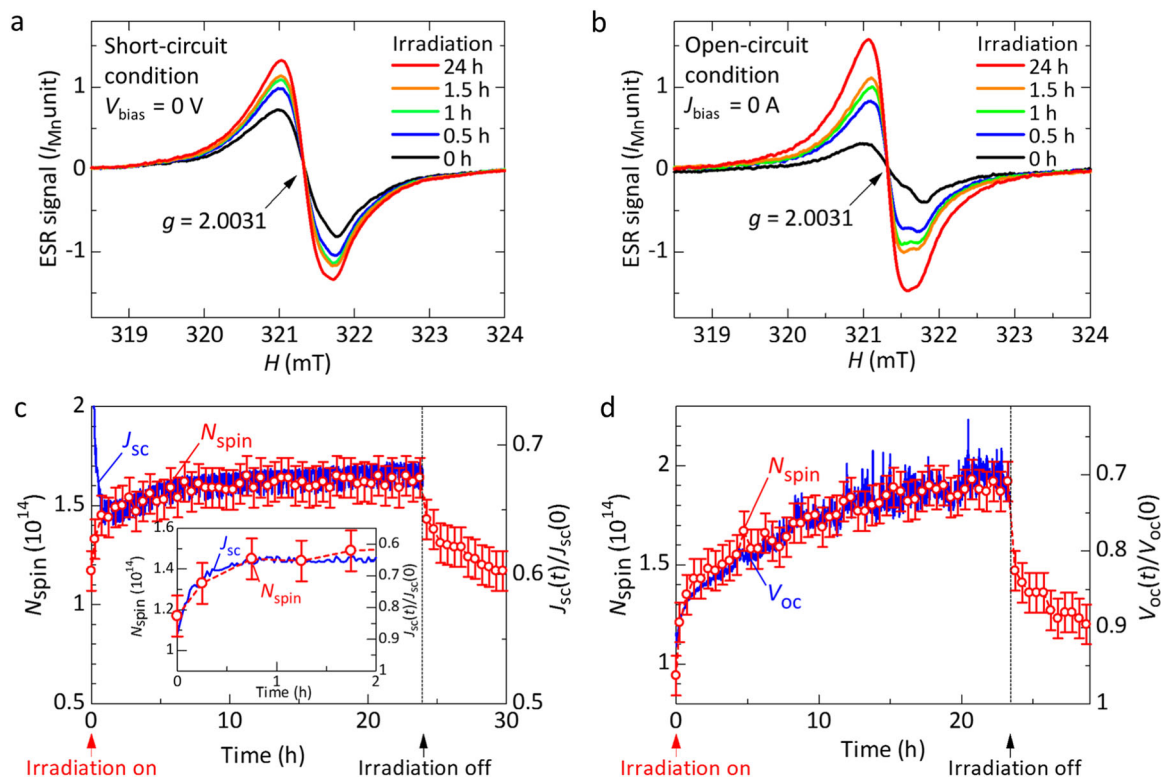
Fig. 2 Operando ESR spectra and the correlation with the device performance. a, b Time variation of ESR spectra of a solar cell (quartz/ITO/compact TiO$_2$/CH$_3$NH$_3$PbI$_3$/spiro-OMeTAD/Au) under simulated solar irradiation on or off at room temperature under short-circuit (**a**) and open-circuit conditions (**b**), respectively. The direction of an external magnetic field (H) is parallel to the substrate plane. The spectra were measured by averaging data under the light irradiation during 30 min. **c, d** Time variation of the number of spins (N_{spin}) (red circle) and short-circuit density (J_{SC}) (blue solid line) (**c**) or open-circuit voltage (V_{OC}) (blue solid line) (**d**) of the cells under simulated solar irradiation on or off at room temperature. The N_{spin} were measured with the averaged ESR spectra under the light irradiation during 30 min, and are plotted at each averaged time over 30 min. The error bars in **c, d** are ±1.0 × 10^{13}.

fabricated to analyze the ESR results of the cells. Figure 1c shows the schematic structure of electrical contacts of Ag pastes and copper wires of the perovskite solar cell in an ESR sample tube, where the wires come out of the sealed tube and connect to a source meter (Keithley, 2612A). Supplementary Fig. 1 shows the current density–voltage (J–V) curves of a fabricated perovskite solar cell. In the present ESR measurements, a continuous wave method with a lock-in detection for an external magnetic field with a 100 kHz modulation frequency was used. Thus, charge carriers with a short lifetime (≤10 μs) contributing to normal device operation is undetectable, and only charges accompanied with spins with a long lifetime (≥10 μs) in the device can be observed. To examine the influence of ultraviolet (UV) rays, we measured the sample under simulated solar irradiation with a filter that cuts short wavelengths of ≤440 nm.

Operando spin observation of perovskite solar cells. It is important for perovskite solar cells to clarify the origin of the deterioration of the device performance, which can be performed by observing the spin states from a microscopic viewpoint, as discussed for study of organic solar cells[22–24]. The long-lived spin states can be clearly observed by ESR measurements. To observe spin states in the internal device during operation and to investigate the correlation with the device performance, the device performance and ESR signals at room temperature under simulated solar irradiation were simultaneously measured. In Fig. 2a, b, we present operando ESR spectra of the perovskite solar cell under simulated solar irradiation, which were measured under short-circuit and open-circuit conditions, respectively. The axis of

ordinates is plotted with a unit of the peak-to-peak ESR intensity (I_{Mn}) of the Mn^{2+} standard sample, where the number of spins of Mn^{2+} is 1.48 × 10^{13}. The ESR signals increased with increasing the duration of simulated solar irradiation. The measured g factors are $g = 2.0031 ± 0.0001$. This g-factor is ascribed to holes with spins in spiro-OMeTAD[25], as described later in details. The ESR-intensity increase represents the accumulation of long-lived holes (lifetime: ≥10 μs), which demonstrates that the hole accumulation occurs in the high-efficient perovskite solar cell under simulated solar irradiation. We have confirmed that the temperature of the device was not changed under light illumination during the ESR measurements. Thus, the ESR-intensity increase is not ascribed to the temperature variation.

Comparing this hole accumulation with the device performance is an interesting issue, which can be conducted by observing the change in the number of spins in the device. The number of charges accompanied with spins, N_{spin}, can be evaluated with the double integration of the ESR spectrum and the comparison of the value with that of the Mn^{2+} marker sample[25]. We will discuss the transient response of the N_{spin} with simulated solar irradiation on or off. Figure 2c, d exhibits the comparison between the N_{spin} and short-circuit current density $J_{SC}(t)/J_{SC}(0)$ or open-circuit voltage $V_{OC}(t)/V_{OC}(0)$ under short-circuit or open-circuit conditions, respectively, which are normalized with the values of the initial state. Under short-circuit conditions, the J_{SC} rapidly decreased and then gradually increased when the N_{spin} increased. However, the V_{OC} monotonically decreased when the N_{spin} increased under open-circuit conditions. As demonstrated by Fig. 2c, d, we have found clear
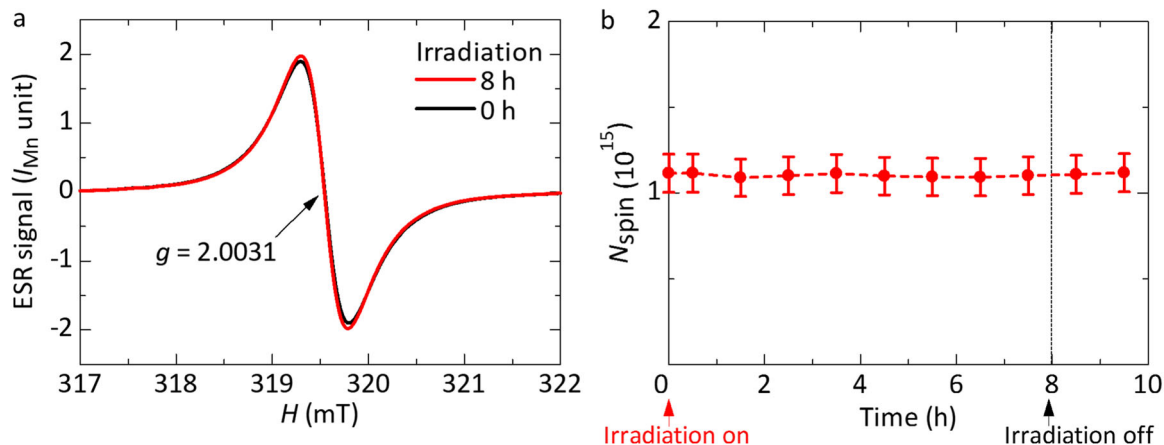
Fig. 3 ESR spectra of an ITO/spiro-OMeTAD layered film. a Time variation of ESR spectra of a quartz/ITO/spiro-OMeTAD layered film under simulated solar irradiation at room temperature, which were measured by averaging data over 1 h. **b** Time variation of the N_{spin} of the layered film under simulated solar irradiation on or off at room temperature. The N_{spin} were obtained with the averaged ESR spectra under the light irradiation for 1 h. Each error bar in **b** is 10% of each measured N_{spin} value, which is approximately 1.1×10^{14}.

correlations between the N_{spin} and changes of the device performance; the detailed correlations will be discussed later.

Origin of spin species in perovskite solar cells. From now on, we discuss the ESR origin for the signal with $g = 2.0031$ shown in Fig. 2a, b, which identifies the layer with charge/spin accumulation. In the ESR measurement of this device, the signals from ITO and Au were not clearly observed, which is because they are thin films with metallic states, that is, Pauli paramagnetic states with lower ESR intensity compared to Curie paramagnetic states due to isolated spin species, and the ESR intensities are below the detection limit of the experiment. In addition, since the spin lattice relaxation times of TiO_2 and $CH_3NH_3PbI_3$ are very short at room temperature, the ESR linewidth of these ESR signals becomes too broad to observe the ESR signal at room temperature[25,26,28,29]. That is, only spiro-OMeTAD's ESR signal can be observed at room temperature. This observation has been reported in the previous study with spiro-OMeTAD films with Li-TFSI dopants, where the ESR signal of holes, in other words, of radical cations or diradical dications, is observed at room temperature[25]. Similarly, it is expected that the ESR signal from holes in spiro-OMeTAD due to FK102 dopants can be observed by ESR measurement. Figure 3a shows the data of a layered film of ITO/spiro-OMeTAD, where ESR signal ($g = 2.0031 \pm 0.0001$) was observed under dark conditions and simulated solar irradiation, respectively. The axis of ordinates is plotted with the I_{Mn} unit using a Mn^{2+} marker sample with the number of spins of 4.16×10^{13}. The observed g value is fully consistent with that reported in the previous studies for spiro-OMeTAD with Li-TFSI or H-TFSI dopants[25,30]. Therefore, it is found that the g factor of $g = 2.0031$ is ascribed to holes formed in the spiro-OMeTAD film doped with Li-TFSI and FK102. From this result, we can identify that the ESR signal of $g = 2.0031$ observed for the device comes from holes in spiro-OMeTAD.

Here, we discuss the doping levels in the spiro-OMeTAD film on the basis of the ESR characteristics. When this layered film was irradiated with simulated solar irradiation for 8 h, the N_{spin} hardly changed as shown in Fig. 3b. In contrast, it has been reported that the N_{spin} increased with increasing the duration of simulated solar irradiation for the spiro-OMeTAD films without or with Li-TFSI doping[25]. In the previous study, the spiro-OMeTAD film was only doped with Li-TFSI[25], whereas the present spiro-OMeTAD

film was doped with FK102 in addition to Li-TFSI. To compare the doping effects between Li-TFST and FK102, we evaluated the doping level from the number of observed spins and that of spiro-OMeTAD molecules in the film. The number of spins is evaluated by the use of the above-mentioned known number of spins of the Mn^{2+} standard marker sample. The number of spiro-OMeTAD molecules is evaluated from the reported density (1.82 g cm^{-3}) of the spiro-OMeTAD thin film[31] and the volume ($1.35 \times 10^{-3} \text{ cm}^3$) of the present spiro-OMeTAD film. As a result, the doping level in the spiro-OMeTAD film with FK102 and Li-TFST dopants is evaluated as 10.6% or 5.3% per a spiro-OMeTAD monomer unit in the cases of radical cations or diradical dications formation, respectively; these values correspond to one radical cation per 9.4 spiro-OMeTAD molecules or one diradical dication per 18.9 spiro-OMeTAD molecules, respectively. The states of spiro-OMeTAD molecules in the film are amorphous, which may cause such high doping level. This value is one order of magnitude higher than 0.90% or 0.45% that have been evaluated for the spiro-OMeTAD film doped with only Li-TFSI[25]. Therefore, we demonstrate at a molecular level that FK102 has a stronger doping effect than Li-TFSI. This result may indicate that the deep trapping levels due to amorphous nature of spiro-OMeTAD are filled by holes due to the FK102 doping, and that the photogenerated charge carriers due to charge separation rapidly recombine without trappings, which may result in the almost unchanged N_{spin} under simulated solar irradiation. If one carefully looks at Fig. 2a, b, one can notice weak structures in these ESR spectra, which may be ascribed to the ESR line broadening due to dipolar coupling between spins from high doping level more than 5%. Such structures have not been observed for spiro-OMeTAD films doped with only Li-TFSI with low doping levels less than 1%[25].

To check experimentally whether charge/spin accumulation didn't occur in layers other than spiro-OMeTAD, low-temperature ESR measurements were performed on the device below 100 K after simulated solar irradiation at room temperature. We have performed a fitting analysis with two components for the observed ESR spectrum, which is shown in Fig. 4. The signal with $g = 2.0009$ (Comp. 1) is ascribed to dangling bonds in the quartz substrate[32], which has been formed by the UV-ozone treatment during substrate cleaning. The signal with $g = 2.0031$ (Comp. 2) is derived from spiro-OMeTAD, as discussed above. Similar result has been obtained from the ESR measurement at 4
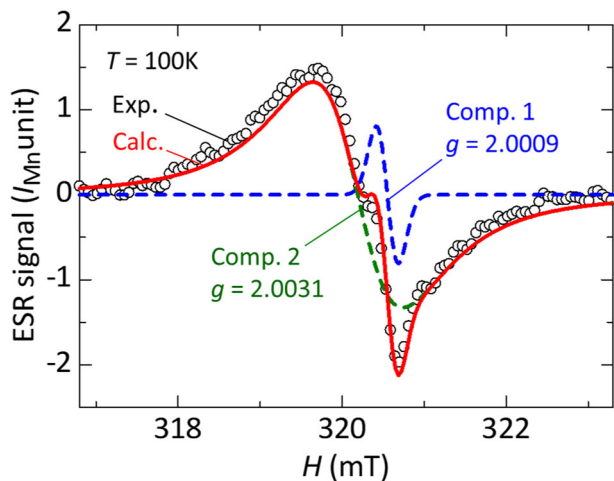
Fig. 4 ESR spectrum and the fitting analysis of the perovskite solar cell at 100 K. ESR spectrum of the cell was observed at 100 K under open-circuit conditions after 20 h simulated solar irradiation at room temperature. The data is explained by a fitting calculation analysis using a least-squares method.

K. Since signals other than spiro-OMeTAD were not observed, we conclude that the charge/spin accumulation only occurs in the spiro-OMeTAD layer. In the following, we compare the N_{spin} in spiro-OMeTAD with the device performance.

We comment on the broader ESR linewidth at low temperatures such as 100 K shown in Fig. 4 compared to the case at room temperature shown in Fig. 2. The reason for the narrowing of the ESR linewidth at high temperatures is ascribed to the effect of the motional narrowing, because the spiro-OMeTAD film is amorphous and has trapping levels for charge/spin carriers. In this case, the motion of charge/spin carriers is enhanced at high temperatures, which narrows the ESR linewidth due to the averaging of hyperfine interactions in the film. We also comment that the reason why the ESR signal with $g = 2.0009$ (Comp. 1) appeared at low temperature (100 and 4.3 K) may be ascribed to a larger saturation effect of the ESR intensity of spiro-OMeTAD (Comp. 2) than that of dangling bonds in the quartz substrate (Comp. 1). That is, ESR signals of organic molecules tend to saturate and show low intensity at low temperatures compared to those of inorganic materials.

Correlation between spin states of spiro-OMeTAD and device performance. We turn to a discussion of the changes of the device performance under device operation from a microscopic viewpoint. As presented in Fig. 2c, the J_{SC} of the cell rapidly decreased (see the inset) and then gradually increased (see the main panel) when the N_{spin} increased under short-circuit conditions. The studies of organic solar cells have reported the J_{SC} decrease due to charge-carrier scatterings by charge accumulation in cells[22,33,34]. When the charge-carrier scatterings occur due to hole accumulation or formation, the current density j of a solar cell may be described with a following equation based on the Matthiessen's rule with charge density (n), electric elemental quantity (e), charge mobility (μ) in the cell, internal electric field (E), charge mobility before (μ_{SC}), and after hole accumulation (μ_{HA}), and a proportional constant (c)[33,34]:

$$j = ne\mu E = ne\frac{\mu_{SC}\mu_{HA}}{\mu_{HA} + (\mu_{SC}/c)N_{spin}}E. \quad (1)$$

In this study, we use the modified expression of j using $\mu(0)$ ($=\mu_{SC}$) and $\mu(N_{spin})$ ($=\mu_{HA}$) as a function of N_{spin}, where $\mu(0)$

and $\mu(N_{spin})$ are the charge mobility in spiro-OMeTAD before and after device operation; the N_{spin} is the number of formed or accumulated holes accompanied with spins. Then, Eq. (1) can be deformed using $\mu(0)$ and $\mu(N_{spin})$ to the following equation:

$$j = ne\frac{\mu(0)}{1 + \left(\frac{\mu(0)}{\mu(N_{spin})c}\right)N_{spin}}E. \quad (2)$$

According to Eq. (1), the j decreases when the N_{spin} increases, which explains the rapid decrease in the J_{SC} observed just after the light irradiation as shown in the inset of Fig. 2c. However, according to Eq. (2), if the $\mu(N_{spin})$ is largely improved from the $\mu(0)$ with N_{spin}, that is, $\mu(N_{spin}) \gg \mu(0)$, the j can increase when the N_{spin} increases. This $\mu(N_{spin})$ improvement explains the gradual J_{SC} increase after 2 h light irradiation as shown in the main panel of Fig. 2c. The charge mobility in spiro-OMeTAD has been reported to be largely improved when the Li-TFSI dopants are added to spiro-OMeTAD[35,36]. In the present study, it is probable that the charge mobility in spiro-OMeTAD is similarly improved by the hole accumulation due to the fillings of deep-trapping levels. Thus, we may conclude from this study that the gradual J_{SC} increase under short-circuit conditions can be explained by the increase in the charge mobility; this result is ascribed to the hole accumulation in spiro-OMeTAD in the solar cell during device operation.

We comment on the J_{SC} variation before and after 2 h light irradiation. The change of the J_{SC} variation after 2 h light irradiation may indicate that the redistribution of hole accumulation in the spiro-OMeTAD film. That is, the sites with hole accumulation in the initial state before 2 h light irradiation may concentrate at the perovskite/spiro-OMeTAD interfaces due to hole transfer from perovskite to spiro-OMeTAD, which may primarily cause the charge-carrier scatterings at around the interfaces. After 2 h light irradiation, the hole-accumulation sites may be redistributed to deep-trapping levels in the spiro-OMeTAD film, which may primarily cause the improvement of charge mobility in the spiro-OMeTAD film, as discussed above.

Next, we discuss the charge/spin states under open-circuit condition. The charge accumulation in the device has been reported to affect the potential distribution in the device[22,37,38]. Under open-circuit conditions as shown in Fig. 2d, the V_{OC} decreased as the hole accumulation increased. The studies of organic solar cells have discussed that when hole accumulation occurs in p-type polymers at the interfaces between photoactive and hole-transport layers, a vacuum-level shift occurs and decreases the V_{OC}[22,33,37]. In this study, it is expected that the V_{OC} decrease is influenced by the shift of the vacuum level owing to accumulated holes at the interfaces between spiro-OMeTAD and gold electrode, because the perovskite layer has no charge accumulation and the electron accumulation in the metallic gold electrode may be unobservable due to the Pauli paramagnetism and the ESR detection limit as mentioned above. It has been argued that when charge accumulation occurs, the variation of the V_{OC} (ΔV_{OC}) is related with the variation of hole accumulation N_{spin} (ΔN_{spin}) using a following equation with an interfacial electric dipole length (d), the permittivity constant in vacuum (ε_0), a dielectric constant of spiro-OMeTAD (ε_r)[39], an area (S) at the spiro-OMeTAD/Au interface in the device as follows[33]:

$$\Delta V_{OC} = \frac{ed}{\varepsilon_0\varepsilon_r S}\Delta N_{spin}. \quad (3)$$

As shown in Eq. (3), the ΔV_{OC} have a proportional relationship with the ΔN_{spin}, which explains the correlation between the N_{spin} and $V_{OC}(t)/V_{OC}(0)$ as shown Fig. 2d. Thus, it is suggested that the charge accumulation at the spiro-OMeTAD/Au interfaces contributes to cause the V_{OC} decrease under open-circuit conditions.
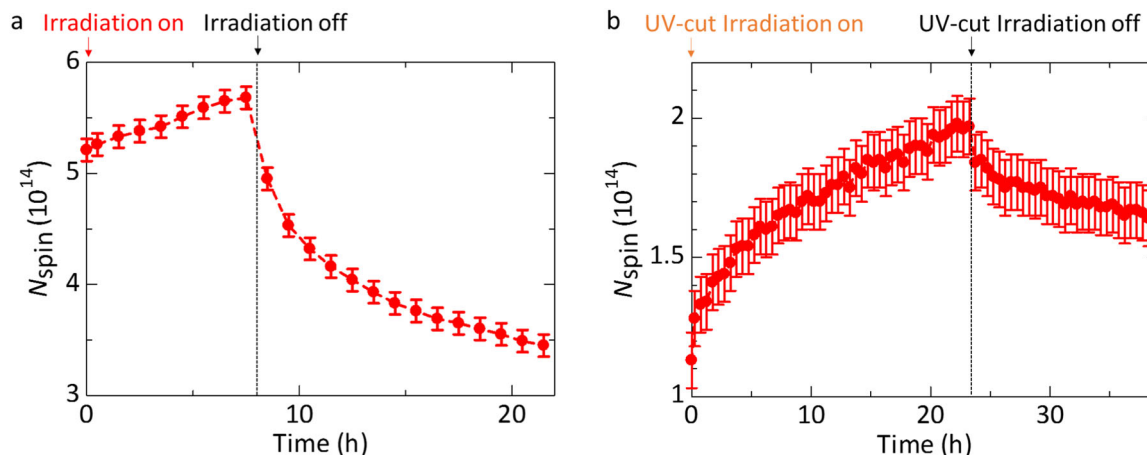
Fig. 5 Effect of UV-light irradiation on a perovskite-solar-cell layered film. a, b Transient response of the N_{spin} of a quartz/ITO/compact TiO$_2$/CH$_3$NH$_3$PbI$_3$/spiro-OMeTAD layered film without Au electrode on simulated solar irradiation (**a**) or on simulated solar irradiation without UV light (**b**) at room temperature. These two measurements were performed on the same layered film. The N_{spin} were measured with the averaged ESR spectra under the light irradiation over 30 min. The error bars in **a**, **b** are ±1.0 × 10^{13}.

In other words, the interfacial electric dipole layer may be formed at the spiro-OMeTAD/Au interfaces.

The above-mentioned direct correlation between the spin states and device performance of the solar cells cannot be obtained from other techniques, such as electrical characterization of devices, impedance measurements, optical spectroscopy, etc., because these techniques cannot directly observe the spin states of perovskite solar cells with high sensitivity and high precision. Thus, we emphasize that we have clearly observed the spin states of perovskite solar cells with high sensitivity and high precision under device operation.

If one carefully looks at Fig. 2d in addition to Fig. 2c, one can notice that the rapid and gradual increases in the N_{spin}. Thus, these results may indicate a distribution of faster and slower processes with nonexponential time evolution. Also, the gradual decreases in the N_{spin} after irradiation off are larger than the gradual increases in the N_{spin} before irradiation off, which may be ascribed to the reverse electron transfer, as will be discussed later. We have used quite generally accepted ideas and formulae in the present work, because we have tried to understand our results as simple as possible. Further study with more complicated modeling seems an interesting topic, such as investigations into the above-mentioned fast and slow dynamics with a model analysis, which are in progress and will be published in a separate paper.

Persistent reverse electron transfer from TiO2 to spiro-OMeTAD under dark conditions. Finally, we discuss the origin of the large N_{spin} decrease of the device after turning off simulated solar irradiation for long duration as shown in Fig. 2c, d. We refer to the overall decay, not the sudden down step, in the N_{spin} after switching off the illumination. To investigate the origin, we studied a layered sample of quartz/ITO/compact TiO$_2$/CH$_3$NH$_3$PbI$_3$/spiro-OMeTAD without gold electrode because the sample is useful to avoid the effect of the interfacial electric dipole layer formed at the spiro-OMeTAD/Au interfaces. The observed result is shown in Fig. 5a, where a large decrease in the N_{spin} has been observed after turning off simulated solar irradiation, as in the case of the device. One of factors for the N_{spin} decrease seems to be ascribed to the recombination of charges which were photogenerated by the charge separation. However, this charge recombination cannot explain the behavior that the N_{spin} decreases further below the initial value obtained before light

irradiation. Thus, the other factor for the decrease may be ascribed to the reverse electron transfer from TiO$_2$ to spiro-OMeTAD by light irradiation (see Fig. 1b)[27,40]. TiO$_2$ is known to release electrons when TiO$_2$ is irradiated with UV light[41]. It has been argued that the reverse electron transfer from TiO$_2$ layer to spiro-OMeTAD layer occurs through voids in the perovskite layer in the solar cells[40].

To confirm the existence of such pin-holes in our perovskite films, we have measured surface images of our film with scanning electron microscope (SEM). An example of the SEM images is shown in Supplementary Fig. 2, which indicates that the surface coverage of a perovskite film fabricated by our method is fairly well. However, one can confirm small pin-holes in the perovskite film, as shown in Supplementary Fig. 2. The pin-holes may be regarded as the main cause of the reverse electron transfer. This reverse electron transfer reasonably explains the decrease in the N_{spin} of holes in spiro-OMeTAD from the initial value after irradiation off shown in Fig. 5a. The spin state of spiro-OMeTAD may be indirectly affected by the film quality of the perovskite, because the reverse electron transfer may be caused by small pin-holes in the perovskite film. Even in this case, our result clearly demonstrates the correlation between the spin state of spiro-OMeTAD and device performance.

To investigate the effect of UV-light irradiation on the N_{spin} decrease, we used an UV-light filter that cuts the light below 440 nm, and compared the change of the N_{spin} under simulated solar irradiation with and without UV light. Figure 5b shows the transient response of the N_{spin} on simulated solar irradiation without UV light. In contrast to the case under simulated solar irradiation with UV light, the N_{spin} did not decrease below the initial value after turning off the irradiation without UV light. Thus, we may conclude that the reverse electron transfer from TiO$_2$ to spiro-OMeTAD occurs in the layered sample and device due to UV light excitation, which explains the reason why the doping concentration in spiro-OMeTAD decreased from that before light irradiation. The finding indicates that the device performance can be kept by preventing the reverse electron transfer through the perovskite layer, in other words, by maintaining the doping effects in spiro-OMeTAD. To restrain the reverse electron transfer, the elimination of voids from perovskite layers and the insertion of electron broking layer between perovskite and spiro-OMeTAD layers would be effective methods. The ESR signals of holes (O$^-$ radicals) in TiO$_2$ can be observed at low temperatures. We have not observed such signals from the ESR measurements even at low temperatures. Thus, the

holes may be transferred from TiO_2 to perovskite according to the energy diagram shown in Fig. 1b.

We comment on the different initial N_{spin} between in Fig. 5a, b. We have performed two measurements of Fig. 5a, b on the same layered film without Au electrode; after measuring the data of Fig. 5a, the data of Fig. 5b was measured using the same film. The reason for the different initial N_{spin} between Fig. 5a, b is that the N_{spin} after taking the data of Fig. 5a largely decreased to the initial N_{spin} in Fig. 5b. This large decrease in the N_{spin} may be ascribed to persistent reverse electron transfer under dark conditions. The process of slow build-up of hole concentration is almost reversible except for the initial value. As shown in Fig. 5a, b, the increase amount of the N_{spin} is approximately 0.5×10^{14} after 8 h light irradiation, which is consistent with each other. The persistent reverse electron transfer under dark conditions may be caused by light-activated ions with a nonmagnetic state that are trapped at trapping sites such as interface, which can cause a difference as compared to dark conditions. For trapping sites of electrons with a nonmagnetic state in TiO_x, the possibility of OH groups in TiO_x has been discussed[23]. In this case, when an OH group can capture an electron and the capture can weaken the bonding between the OH group and Ti, an ESR-inactive OH^- ion can be formed under UV-light irradiation[23]. Since the process is reversible, the OH^- ion may be electrostatically captured nearby Ti, which may be expressed as $\equiv Ti - OH + e^- \rightarrow \equiv Ti \cdots OH^-$ where the dotted line "$\cdots$" and three solid lines "$\equiv$" represent an electrostatic capture and three Ti–O bonds with other three oxygen atoms, respectively. One electron of Ti used for the Ti–OH bond may be delocalized or included in TiO_x bands after the electron capture, and could not be detected by ESR because of the degenerate states, that is, Pauli paramagnetic states with lower ESR intensity compared to Curie paramagnetic states, as discussed in the cases of the ITO and Au electrodes mentioned above. This $\equiv Ti \cdots OH^-$ is an UV-light-activated ion with a nonmagnetic state, and this nonmagnetic state is consistent with the non-observation of ESR signal except for spiro-OMeTAD, as discussed above. Such electron trapping may be an origin of the persistent reverse electron transfer under dark conditions.

Similar result has been observed for the solar cell shown in Fig. 2. We have performed two experiments on the same device for the correlation with J_{SC} and V_{OC} shown in Fig. 2. After performing the experiment under short-circuit conditions shown in Fig. 2a, c, we have performed the experiment under open-circuit conditions shown in Fig. 2b, d. The memory effect cannot be completely avoided, in particular, for the N_{spin}. This is because the N_{spin} strongly depends on the previous light illumination, which may be due to the persistent reverse electron transfer, as mentioned above. If one carefully looks at the initial value of the N_{spin} shown in Fig. 2, one can notice that the initial value shown in Fig. 2d is smaller than that in Fig. 2c; this decrease may be explained by the above-mentioned persistent reverse electron transfer.

A study of $CH_3NH_3PbI_3$/spiro-OMeTAD layered films with transient absorption and emission spectroscopies has reported that the carrier recombination between the interface layer spiro-OMeTAD and the perovskite layer varies with respect to light intensities within a time scale of 300 ns[42]. This time scale is much shorter than that discussed in our study (several tens of hours), and such fast carrier recombination cannot be observed by the present continuous-wave ESR method because of the time resolution of ≥ 10 μs. Thus, the present ESR signals are not correlated to the carrier recombination in the fast time scale of ≤ 10 μs. We have not measured the dependence of the ESR intensity on the light intensity, which seems an interesting issue and will be discussed in a separate study.

Conclusion

We have directly investigated the spin states in the perovskite solar cells at the molecular level during device operation under simulated solar irradiation. Operando ESR spectroscopy demonstrates that the change of the doping states in the HTL spiro-OMeTAD varies not only the J_{SC} due to charge-carrier scatterings and charge-mobility improvements under short-circuit conditions but also the V_{OC} due to the formation of interfacial electric dipole layer under open-circuit conditions. Our results have shown the clear correlation between the number of spins in the cells and the device performance. Also, we have proved from the microscopic viewpoint that the following points are important to prevent the device-performance degradation: (1) the improvement of the charge mobility in spiro-OMeTAD, which can be performed by increasing the doping levels due to deep-trap fillings without large charge-carrier scatterings, and (2) the prevention of the formation of the interfacial electric dipole layer in the device. In addition, it has been directly demonstrated at the molecular level that the reverse electron transfer from TiO_2 layer to spiro-OMeTAD layer occurs through the perovskite layer by UV-light irradiation. Since this reverse electron transfer causes the decrease in the doping levels in spiro-OMeTAD in the device, the prevention of the reverse electron transfer in perovskite layers is essential not only to decrease the leakage current but also to maintain the spiro-OMeTAD doping effects. Thus, the present operando spin analysis of solar cells from a microscopic view-point would be useful to obtain further detailed information about the operation and degradation mechanism, which may give a new guideline for improving the device performance and durability, and also be useful for other perovskite solar cells.

Methods

Device fabrication. Compact TiO_2 was fabricated by a sputtering on quartz/ITO substrate which was cleaned by UV ozone. $PbCl_2$ (0.2464 g), methylammonium iodide (MAI, 0.4259 g), and N,N-dimethylformamide (DMF, 1.0 mL) were mixed as a perovskite solution with the 1:3 mixture ratio of $PbCl_2$:MAI in DMF solvent (0.8 M) (see ref. [3]), which was stirred for 3 h in a nitrogen-filled glove box (O_2 of <0.2 ppm, H_2O of <0.5 ppm). Thereafter, the solution was filtered and spin-coated on compact TiO_2, stored in the glove box for 30 min, and annealed at 90 °C for 3 h to form a perovskite layer in the glove box. As a solution of HTM, spiro-OMeTAD (73.0 mg), a lithium salt lithium bis(trifluoromethanesulfonyl)imide (Li-TFSI, 9.2 mg), a solvent 4-tert-butylpyridine (TBP, 28.8 μL), a cobalt complex tris(1-(pyr-idin-2-yl)-1H-pyrazol)cobalt(II) bis(hexafluorophosphate) (FK102, 8.7 mg), and chlorobenzene (1 mL) were mixed and stirred. Li-TFSI, TBP, and FK102 were used as dopants for improving device performance[27]. The solution was filtered and spin-coated on the perovskite layer, and then dried at 75 °C for 30 min to form a spiro-OMeTAD layer. Finally, a gold electrode was formed by a vacuum evaporation method. After fabricating the device, it was inserted into an ESR sample tube and then sealed in the glove box.

ESR spectroscopy characterization. ESR measurements were performed with an X-band ESR spectrometer (JEOL RESONANCE, JES-FA200) under dark conditions or simulated solar irradiation with a solar simulator (Bunkoukeiki, OTEN-TOSUN-150LX; AM1.5, 100 mW cm^{-2}). The illumination with the solar simulator happens inside the ESR cavity resonator. The effective illumination intensity on a sample is 100 mW cm^{-2}, which has been previously determined on the position of the sample inside an ESR sample tube with a silicon photodiode. The output of the silicon photodiode has been calibrated with the solar simulator. The ESR parameters, g factor, ESR linewidth, and the number of spins, were calibrated with a Mn^{2+} standard marker. The measured temperatures were between 4 K and room temperature. The parts of the above-mentioned ESR spectroscopy characterization method have been described in the previous works[22–26,37,38,43].

Data availability

References

1. Kojima, A., Teshima, K., Shirai, Y. & Miyasaka, T. Organometal halide perovskites as visible-light sensitizers for photovoltaic cells. *J. Am. Chem. Soc.* **131**, 6050–6051 (2009).
2. Lee, M. M., Teuscher, J., Miyasaka, T., Murakami, T. N. & Snaith, H. J. Efficient hybrid solar cells based on meso-superstructured organometal halide perovskites. *Science* **338**, 643–647 (2012).
3. You, J. et al. Moisture assisted perovskite film growth for high performance solar cells. *Appl. Phys. Lett.* **105**, 183902-1-5 (2014).
4. Park, N.-G. Perovskite solar cells: an emerging photovoltaic technology. *Mater. Today* **18**, 65–72 (2015).
5. Giordano, F. et al. Enhanced electronic properties in mesoporous TiO₂ via lithium doping for high-efficiency perovskite solar cells. *Nat. Commun.* **7**, 10379-1-6 (2016).
6. Tan, Z.-K. et al. Bright light-emitting diodes based on organometal halide perovskite. *Nat. Nanotechnol.* **9**, 687–692 (2014).
7. Li, J. et al. Single-layer halide perovskite light-emitting diodes with sub-band gap turn-on voltage and high brightness. *J. Phys. Chem. Lett.* **7**, 4059–4066 (2016).
8. Chin, X. Y., Cortecchia, D., Yin, J., Bruno, A. & Soci, C. Lead iodide perovskite light-emitting field-effect transistor. *Nat. Commun.* **6**, 7383-1-9 (2015).
9. Matsushima, T. et al. Intrinsic carrier transport properties of solution-processed organic–inorganic perovskite films. *Appl. Phys. Express* **10**, 024103-1-4 (2017).
10. Green, M. A. et al. Solar cell efficiency tables (Version 56). *Prog. Photovolt. Res. Appl.* **28**, 629–638 (2020).
11. Noh, J. H., Im, S. H., Heo, J. H., Mandal, T. N. & Seok, S. I. Chemical management for colorful, efficient, and stable inorganic–organic hybrid nanostructured solar cells. *Nano Lett.* **13**, 1764–1769 (2013).
12. Ogomi, Y. et al. CH₃NH₃SnₓPb₍₁₋ₓ₎I₃ perovskite solar cells covering up to 1060 nm. *J. Phys. Chem. Lett.* **5**, 1004–1011 (2014).
13. Stranks, S. D. et al. Electron-hole diffusion lengths exceeding 1 micrometer in an organometal trihalide perovskite absorber. *Science* **342**, 341–344 (2013).
14. Frost, J. M. et al. Atomistic origins of high-performance in hybrid halide perovskite solar cells. *Nano Lett.* **14**, 2584–2590 (2014).
15. Han, Y. et al. Degradation observations of encapsulated planar CH₃NH₃PbI₃ perovskite solar cells at high temperatures and humidity. *J. Mater. Chem. A* **3**, 8139–8147 (2015).
16. Bryant, D. et al. Light and oxygen induced degradation limits the operational stability of methylammonium lead triiodide perovskite solar cells. *Energy Environ. Sci.* **9**, 1655–1660 (2016).
17. Yin, G. et al. Enhancing efficiency and stability of perovskite solar cells through Nb-doping of TiO₂ at low temperature. *ACS Appl. Mater. Interfaces* **9**, 10752–10758 (2017).
18. Eames, C. et al. Ionic transport in hybrid lead iodide perovskite solar cells. *Nat. Commun.* **6**, 7497-1-8 (2015).
19. Marumoto, K., Kuroda, S., Takenobu, T. & Iwasa, Y. Spatial extent of wave functions of gate-induced hole carriers in pentacene field-effect devices as investigated by electron spin resonance. *Phys. Rev. Lett.* **97**, 256603-1-4 (2006).
20. Matsui, H., Hasegawa, T., Tokura, Y., Hiraoka, M. & Yamada, T. Polaron motional narrowing of electron spin resonance in organic field-effect transistors. *Phys. Rev. Lett.* **100**, 126601-1-4 (2008).
21. Sakanoue, T. et al. High current injection into dynamic p–n homojunction in polymer light-emitting electrochemical cells. *Adv. Mater.* **29**, 1606392-1-7 (2017).
22. Nagamori, T. & Marumoto, K. Direct observation of hole accumulation in polymer solar cells during device operation using light-induced electron spin resonance. *Adv. Mater.* **25**, 2362–2367 (2013).
23. Son, D., Kuwabara, T., Takahashi, K. & Marumoto, K. Direct observation of UV-induced charge accumulation in inverted-type polymer solar cells with a TiOₓ layer: microscopic elucidation of the light-soaking phenomenon. *Appl. Phys. Lett.* **109**, 133301-1-5 (2016).
24. Marumoto, K., Fujimori, T., Ito, M. & Mori, T. Charge formation in pentacene layers during solar-cell fabrication: direct observation by electron spin resonance. *Adv. Energy Mater.* **2**, 591–597 (2012).
25. Namatame, M. et al. Direct observation of dramatically enhanced hole formation in a perovskite-solar-cell material spiro-OMeTAD by Li-TFSI doping. *Appl. Phys. Lett.* **110**, 123904-1-5 (2017).
26. Gotanda, T. et al. Direct observation of charge transfer at the interface between PEDOT:PSS and perovskite layers. *Appl. Phys. Express* **12**, 041002-1-4 (2019).
27. Noh, J. H. et al. Nanostructured TiO₂/CH₃NH₃PbI₃ heterojunction solar cells employing spiro-OMeTAD/Co-complex as hole-transporting material. *J. Mater. Chem. A* **1**, 11842–11847 (2013).
28. Chiesa, M., Paganini, M. C., Livraghi, S. & Giamello, E. Charge trapping in TiO₂ polymorphs as seen by electron paramagnetic resonance spectroscopy. *Phys. Chem. Chem. Phys.* **15**, 9435–9447 (2013).
29. Shkrob, I. A. & Marin, T. W. Charge trapping in photovoltaically active perovskites and related halogenoplumbate compounds. *J. Phys. Chem. Lett.* **5**, 1066–1071 (2014).
30. Abate, A. et al. Protic ionic liquids as p-dopant for organic hole transporting materials and their application in high efficiency hybrid solar cells. *J. Am. Chem. Soc.* **135**, 13538–13548 (2013).
31. Ding, I.-K. et al. Pore-filling of spiro-OMeTAD in solid-state dye sensitized solar cells: quantification, mechanism, and consequences for device performance. *Adv. Funct. Mater.* **19**, 2431–2436 (2009).
32. Giordano, L., Sushko, P. V., Pacchioni, G. & Shluger, A. L. Optical and EPR properties of point defects at a crystalline silica surface: ab initio embedded-cluster calculations. *Phys. Rev. B* **75**, 024109-1-9 (2007).
33. Marumoto, K. & Nagamori, T. Correlation between hole accumulation and deterioration of device performance in polymer solar cells as investigated by light-induced electron spin resonance. *Mol. Cryst. Liq. Cryst.* **597**, 29–32 (2014).
34. Liu, D. et al. Dramatic enhancement of fullerene anion formation in polymer solar cells by thermal annealing: direct observation by electron spin resonance. *Appl. Phys. Lett.* **104**, 243903-1-5 (2014).
35. Snaith, H. J. & Grätzel, M. Enhanced charge mobility in a molecular hole transporter via addition of redox inactive ionic dopant: implication to dye-sensitized solar cells. *Appl. Phys. Lett.* **89**, 262114-1-3 (2006).
36. Abate, A. et al. Lithium salts as "redox active" p-type dopants for organic semiconductors and their impact in solid-state dye-sensitized solar cells. *Phys. Chem. Chem. Phys.* **15**, 2572–2579 (2013).
37. Kubodera, T. et al. Operando direct observation of charge accumulation and the correlation with performance deterioration in PTB7 polymer solar cells. *ACS Appl. Mater. Interfaces* **10**, 26434–26442 (2018).
38. Rachmat, V. A. S. A., Kubodera, T., Son, D., Cho, Y. & Marumoto, K. Molecular oriented charge accumulation in high-efficiency polymer solar cells as revealed by operando spin analysis. *ACS Appl. Mater. Interfaces* **11**, 31129–31138 (2019).
39. Jiménez-López, J., Cambarau, W., Cabau, L. & Palomares, E. Charge injection, carriers recombination and HOMO energy level relationship in perovskite solar cells. *Sci. Rep.* **7**, 6101-1-10 (2017).
40. Shen, Q. et al. Charge transfer and recombination at the metal oxide/CH₃NH₃PbClI₂/spiro-OMeTAD interfaces: uncovering the detailed mechanism behind high efficiency solar cells. *Phys. Chem. Chem. Phys.* **16**, 19984–19992 (2014).
41. Maeda, K. Photocatalytic water splitting using semiconductor particles: history and recent developments. *J. Photochem. Photobiol. C* **12**, 237–268 (2011).
42. Makuta, S. et al. Photo-excitation intensity dependent electron and hole injections from lead iodide perovskite to nanocrystalline TiO₂ and spiro-OMeTAD. *Chem. Commun.* **52**, 673–676 (2016).
43. Xue, D., Kamiya, S., Saito, M., Osaka, I. & Marumoto, K. Direct evidence of less charge accumulation in highly durable polymer solar cells using operando ESR spectroscopy. *ACS Appl. Energy Mater.* **3**, 2028–2036 (2020).

Author contributions

K.M. and T.Y. planned the study. T.Y., T.W., and K.M. fabricated the cells, and measured and analyzed the data. T.W. and K.M. wrote the paper. All authors discussed the results and reviewed the manuscript.

Competing interests

The authors declare no competing interests.

Additional information

Supplementary information is available for this paper at https://doi.org/10.1038/s43246-020-00099-7.

Correspondence and requests for materials should be addressed to K.M.

Peer review information Primary handling editor: Aldo Isidori.

Reprints and permission information is available at http://www.nature.com/reprints

Publisher's note Springer Nature remains neutral with regard to jurisdictional claims in published maps and institutional affiliations.